Journal of Chromatography A, 1217 (2010) 6350–6365

Contents lists available at ScienceDirect

Journal of Chromatography A

journal homepage: www.elsevier.com/locate/chroma

Relationship between trans-column eddy diffusion and retention in liquid chromatography: Theory and experimental evidence

Fabrice Gritti, Georges Guiochon*

Department of Chemistry, University of Tennessee, Knoxville, TN 37996-1600, USA

ARTICLE INFO

Article history:
Received 15 March 2010
Received in revised form 18 June 2010
Accepted 13 July 2010
Available online 23 July 2010

Keywords:
Packed column
Mass transfer resistance
Eddy diffusion
Trans-column eddy diffusion
Trans-column velocity biases
Local electrochemical detection
Benzoquinone
HETP
Uracil
Acetophenone
Toluene
Naphthalene
Core–shell particles
Kinetex-C_{18}

ABSTRACT

Experimental results demonstrate that trans-column eddy diffusion depends on the retention of compounds. The combination of elution profiles recorded in different points of the exit column cross-section and of the height equivalent to a theoretical plate (HETP) of small molecules clearly show a strong link between retention and column performance in liquid chromatography. These results validate a new model of trans-column eddy diffusion in packed columns. The contribution to the column HETP of the trans-column eddy diffusion term decreases with increasing retention factor from $k' = 0$ to $k' = 3$ above which it becomes negligible. The best column performance in RPLC is observed for the most retained compounds. This is due to the combination of the lack of a residual trans-column eddy diffusion contribution and the vanishing contribution of the instrument to band broadening.

1. Introduction

The contribution of eddy diffusion to the efficiency of packed columns was recently shown to depend on whether access to the mesoporous volume of the particles is possible or not [1,2]. The eddy diffusion term for a non-retained compound is typically twice larger when its molecules do not have access to the internal porous volume of the particles than when they can diffuse through it [3]. This result is important because these eddy diffusion terms were measured for the same column, with a constant spatial distribution of the particles inside the column, by successively allowing or blocking access of molecules to the mesopores. Access to the mesopores is blocked by filling them with liquid n-nonane [4]; it is restored by washing nonane off. While it is generally believed that eddy diffusion is independent of whether the particles are porous or not, these observations prove the opposite.

Eddy diffusion provides an important contribution to column efficiency. It is due to the complexity of the structure of the mobile phase stream percolating through the anastomosed network of channels found between the irregularly packed particles. The irregular distribution of the streamlet velocities along this intricate network of channels causes important velocity biases, resulting in an irregular distribution of the solute concentration, hence in steep axial and radial concentration gradients. For a given column, the distribution of these velocity biases is the same whether access to the mesopores is blocked or not.

Giddings described two exchange mechanisms allowing the transfer of molecules from one eluent streamline to another [5]. The first mechanism is governed by the complex flow pattern of these streamlines through the three-dimensional structure of the packed column. The velocity of a molecule changes when it jumps from one streamline to another one. This mechanism applies mainly at high velocities but it ignores the possibility for molecules to be transferred between near streamlines by diffusion. This second exchange mechanism applies mainly at low velocities, when the transfer of the molecules is faster by diffusion than by flow exchange.

Trans-column velocity biases are due to the radially heterogeneous structure of the packed bed, caused by friction between

* Corresponding author at: University of Tennessee, Department of Chemistry, 552 Buehler Hall, Knoxville, TN 37996-1600, USA. Tel.: +1 865 974 0733; fax: +1 865 974 2667.
E-mail address: guiochon@utk.edu (G. Guiochon).

0021-9673/$ – see front matter © 2010 Elsevier B.V. All rights reserved.
doi:10.1016/j.chroma.2010.07.029

particles and between particles and wall during the packing process [6]. The concentration gradients in a column relax differently depending on whether the bed is made of porous or non-porous particles, because the radial dispersion coefficients of solutes in these beds differ [7]. When the particles are non-porous, the apparent radial diffusion coefficient is $\gamma_e D_m + (1/2)\gamma_r u d_p$, with $\gamma_e \simeq 0.6$ the external obstruction factor [8], $\gamma_r \simeq 0.3$ a coefficient accounting for the contribution of flow to transverse dispersion [9,10] and u is the interstitial linear velocity. When the particles are porous, the solute molecules can diffuse either through the interstitial volume ($\gamma_e D_m$) or through the porous particles, with D_{eff}. Furthermore, the time spent by the solute zone in the column is longer when the pores are not blocked, therefore the radial concentration gradients are more effectively relaxed in this configuration.

The goal of this work is to test experimentally these new theoretical considerations regarding eddy diffusion in chromatographic columns. Since earlier approaches cannot account for our new results that prove lower short-range inter-channel and/or trans-column eddy diffusion terms when the particle mesopores are open than when they are blocked [1–3], a different physical interpretation and new models of eddy diffusion are necessary. We report on results of simultaneous measurements of the elution times of a low molecular weight compound, para-benzoquinone, at the center and at the wall of the outlet of a 4.6 mm × 100 mm column in RPLC, when it is eluted with mobile phases of different compositions, giving retention factors between 0 and 3. The trans-column eddy diffusion term was also measured for four compounds with retention factors between 0 and 2.2. These experimental results illustrate the impact of retention on the performance of RPLC columns and on mass transfer kinetics.

2. Theory

2.1. Theory of eddy dispersion in packed columns

Fifty years ago, in his coupling theory of eddy diffusion, Giddings proposed the following general equation to account for the overall eddy diffusion term in packed columns and combined a diffusion and a flow exchange mechanism for each one of four sources i of velocity biases [5]:

$$A = \sum_{i=1}^{i=3} \frac{1}{(1/2\lambda_i) + (1/\omega_i \nu)} \tag{1}$$

In this equation, the index i refers to the type of velocity bias considered in the column, l_i is its characteristic length, along which flow heterogeneities persists in the column, and λ_i and ω_i are empirical parameters. The main velocity biases identified by Giddings, which are still important in modern packed chromatographic columns are the trans-channel ($i = 1$, $l_1 \simeq (d_p/6)$), the short-range inter-channel ($i = 2$, $l_2 \simeq d_p$), and the trans-column ($i = 3$, $l_3 \simeq (d_c/2)$) velocity biases.

The values of the empirical parameters first estimated and physically justified by Giddings are $\lambda_1 = 0.5$, $\omega_1 = 0.01$, $\lambda_2 = 0.5$, and $\omega_2 = 0.5$ [5]. Today, these estimates are still qualitatively valid, even for columns packed with very fine totally porous particles. Recent determinations made for shell particles by combining results of measurements of the radial flow distribution across the exit cross-section of the column [11,12] with the HETP data obtained for columns with access to the mesoporous volume blocked or unblocked gave $\lambda_2 = 0.2$, and $\omega_2 = 0.2$ [2,3,13].

The parameters λ_3 and ω_3 were determined [3,13] by assuming that the radial flow profile, $u(x)$, is given by a polynomial distribution as observed by Farkas et al. [11]:

$$u(x) = u(0)[1 - \omega^*_{\beta,c} x^n] \tag{2}$$

where $\omega^*_{\beta,c}$ is the relative flow velocity difference measured between the center and the wall of the column, n is the polynomial order (n can vary between 2 and 16, depending on the radial extent of the flow uniformity in the center region of the column), x is the dimensionless radial coordinate $x = (r/r_c)$, and $u(0)$ is the velocity at the center of the column ($x = 0$).

Accordingly, λ_3 is written [3]:

$$\lambda_3 = \frac{p}{q}\frac{L}{d_p}\omega^{*,2}_{\beta,c} \tag{3}$$

where L is the column length, d_p the particle diameter, p and q two integers, and $\omega^*_{\beta,c}$, a parameter that cannot be directly measurable at the column outlet, due to the effects of radial dispersion, but can only be underestimated. $\omega^*_{\beta,c}$ could be measured directly if solutes could absolutely not disperse radially across the column, which would eventually relaxes radial concentration gradients. The ratio p/q is equal to 2/45, 8/225, 32/1377, and 128/9537 for $n = 4$, 8, 16, and 32, respectively.

The parameter ω_3 was derived using an extension of the general Aris theory of dispersion in open cylindrical tubes to packed chromatographic beds [14,15]. Accordingly, ω_3 was written [13]:

$$\omega_3 = \frac{A_0 \varepsilon_e}{\varepsilon_e \gamma_e + (1 - \varepsilon_e)(1 - \rho^3)\Omega} \frac{d_c^2}{d_p^2} \tag{4}$$

where A_0 is a parameter calculated after the radial profile distributions of the dispersion coefficient ($D_r(x)$) and of the migration linear velocity of the zone considered, ($u(x)$), across the column [15], d_c is the column diameter, ρ the ratio of the core to the particle diameters for superficially porous particles and Ω the ratio of the solute diffusivity in the shell to that in the bulk mobile phase [16]:

$$\Omega = \varepsilon_{p,shell}\gamma_{p,shell}\left[F(\lambda_m) + \alpha K_{shell}\frac{D_S}{D_m}\right] \tag{5}$$

where $F(\lambda_m)$ is the hindrance diffusion factor of the solute, α the pore/solid structural parameter [16] and D_S/D_m the ratio of the surface diffusion coefficient to the bulk diffusion coefficient. According to Ref. [17], this ratio is reasonably approximated by:

$$\frac{D_S}{D_m} = \frac{1}{1 + 0.7K_{shell}} \tag{6}$$

The radial dispersion coefficient is expressed as the sum of a diffusion (D_0) and a convection (D_{eddy}) terms [3,7]:

$$D_r(x) = D_0 + D_{eddy}(x) = \frac{\varepsilon_e\gamma_e + (1 - \varepsilon_e)(1 - \rho^3)\Omega}{\varepsilon_t(1 + k')} D_m + \frac{1}{2}\gamma_r u(x) d_p \tag{7}$$

where γ_r is a constant smaller than 1 which measures the contribution of eddy diffusion to the transversal dispersion of the solute. γ_r was found to be 0.32, based on NMR experiments [9]. Note that in Eq. (7), the diffusion term, D_0, includes the contribution of the sample diffusivity in the porous shell, $(1 - \varepsilon_e)(1 - \rho^3)\Omega$.

According to Eq. (7), the radial dispersion coefficient for non-porous particles ($\varepsilon_e = \varepsilon_t$, $\rho = 1$, and $\Omega = k' = 0$) is written as:

$$D_r(x) = \gamma_e D_m + \frac{1}{2}\gamma_r u(x) d_p \tag{8}$$

This equation is the application of the general Eq. (7) in this particular case.

2.2. Trans-column eddy dispersion term in a packed column

In this section, we derive a new expression for the trans-column eddy diffusion term ($i = 3$), which is valid for both porous and solid particles.

2.2.1. Diffusion exchange mechanism

When the flow velocity is very small, analyte molecules have enough time to sample the whole column cross-section. The general dispersion theory of Aris [14] in open circular tubes can then be extended to the problem of trans-column eddy diffusion in packed columns. The corresponding reduced HETP term is written [15]:

$$h_{transcolumn,Aris} = C_m \frac{\varepsilon_e}{\varepsilon_t} \frac{d_c^2}{d_p^2} \frac{D_m}{D_r} \frac{1}{1+k'} \nu \quad (9)$$

where C_m is a constant derived from the radial velocity profile, $u(x)$, as follows [15]:

$$C_m \frac{D_0}{D_r} = A_0 \quad (10)$$

with

$$A_0 = \frac{I_1 - 2I_2 + I_3}{2} \quad (11)$$

and

$$I_1 = \int_0^1 \frac{\Phi^2(x)}{2x\Psi(x)} dx \quad (12)$$

$$I_2 = \int_0^1 \frac{x\Phi(x)}{2\Psi(x)} dx \quad (13)$$

$$I_3 = \int_0^1 \frac{x^3}{2\Psi(x)} dx \quad (14)$$

with

$$\Phi(x) = \int_0^x 2x'\phi(x')dx' \quad (15)$$

In these equations, x' is a dummy variable. The functions $\phi(x)$ and $\psi(x)$ are the dimensionless radial profiles of the linear migration velocity of the zone, u, and of the radial diffusion coefficient D_r, respectively [14,18]. In the particular case discussed here:

$$\phi(x) = \frac{u_R(x)}{u_R} = \frac{u_R(x)}{2\int_0^1 u_R(x')x'dx'} \quad (16)$$

and

$$\Psi(x) = \frac{D_r(x)}{D_0} \quad (17)$$

2.2.2. Flow exchange mechanism

When the flow velocity is large, in contrast, the radial dispersion of the sample is no longer effective to relax radial concentration gradients. Then, band broadening is directly related to the radial flow distribution across the column. For the sake of illustration, assume a radial flow velocity profile distribution with $n = 12$ in Eq. (2); the linear velocity flow profile, $u(x)$, is then written [11]:

$$u(x) = u(0)[1 - \omega^*_{\beta,c} x^{12}] \quad (18)$$

The corresponding reduced HETP is then [3,19]:

$$h_{transcolumn,Flow} = 2\lambda_3 = \frac{36}{637} \frac{L}{d_p} \omega^{*2}_{\beta,c} \quad (19)$$

2.2.3. Giddings's coupling theory of eddy diffusion

In most cases, under normal experimental conditions, neither a pure diffusion model nor a pure flow mechanism can account for the experimental data. Eventually, both mechanisms participate simultaneously to the trans-column band broadening of the sample. This is the basis of the general theory of Aris [14] regarding mass transfer along tubes of any cross-section geometry, which simultaneously accounts for the axial flow heterogeneity and the radial sample dispersion. According to the general coupling equation of Giddings 1:

$$h_{\text{trans-column}} = \frac{1}{(1/h_{\text{trans-column,Aris}}) + (1/h_{\text{trans-column,Flow}})} \quad (20)$$

Therefore, if we assume $n = 12$, the trans-column eddy diffusion term is written:

$$h_{\text{trans-column}} = \frac{1}{(\varepsilon_e\gamma_e + (1-\varepsilon_e)(1-\rho^3)\Omega/\varepsilon_e A_0)(d_p^2/d_c^2)(1/\nu) + (637/36)(d_p/L)(1/\omega^{*,2}_{\beta,c})} \quad (21)$$

Table 1
Physico-chemical properties of the two Kinetex columns used in this work given by the manufacturer and measured in our lab[a,b,c,d].

Neat silica	Kinetex (1)	Kinetex (2)
Particle size [μm]	2.5	2.5
$\rho = R_i/Re$[a]	0.75	0.75
Pore diameter [Å]	92	85
Surface area [m/g]	100	100
Particle size distribution ($d_{90\text{-}10\%}$)	1.1	1.1
Bonded phase analysis	Kinetex-C18 (1)	Kinetex-C18 (2)
Total carbon [%]	6	6
Surface coverage [μmol/m^2]	2.7	2.7
Endcapping	Yes	Yes
Packed columns analysis	Column (1)	Column (2)
Lot number/serial number	5569-76/496449-7	5569-120/520795-42
Dimension (mm × mm)	4.6 × 100	4.6 × 100
External porosity[b]	0.40	0.41
Total porosity[c]	0.53	0.52
Particle porosity[d]	0.22	0.19
Shell porosity	0.37	0.32

[a] Measured from Coulter counter technique (30,000 particles).
[b] Measured by inverse size exclusion chromatography (polystyrene standards).
[c] Measured by pycnometry (IPrOH–CH_2Cl_2).
[d] The particle porosity includes the volume of the solid silica core.

3. Experimental

3.1. Chemicals

The mobile phases used in this work were aqueous mixtures of methanol or acetonitrile. Dichloromethane ($\rho_{CH_2Cl_2} = 1.323$ g/cm^3) and tetrahydrofuran ($\rho_{THF} = 0.883$ g/cm^3) were used in markedly smaller amounts to measure the column hold-up volumes by pycnometry. These five solvents were HPLC grade from Fisher Scientific (Fair Lawn, NJ, USA). The mobile phase was filtered before use on a surfactant-free cellulose acetate filter membrane, 0.2 μm pore size (Suwannee, GA, USA). Para-benzoquinone, fructose, and potassium chloride were purchased from Aldrich (Milwaukee, WI, USA). The sample mixture, containing uracil, acetophenone, toluene, and naphthalene dissolved in pure acetonitrile, was provided by Phenomenex (Torrance, CA, USA).

3.2. Columns

Two 100 × 4.6 mm columns packed with 2.5 μm Kinetex-C_{18} (columns 1 and 2) were generous gifts from their manufacturer (Phenomenex, Torrance, CA, USA). The main characteristics of the bare porous silica and those of the final derivatized packing material are summarized in Table 1. They are virtually identical.

3.3. Micro-electrodes and columns' modification

In order to perform the local electrochemical detection (LED) experiments appropriately, one end of the columns was modified to allow local oxidation of para-benzoquinone (+0.7 V *versus* Ag/AgCl)

and fructose (+0.9 V *versus* Ag/AgCl) at the tip of a home-made micro-electrode located at a distance r from the center of the outlet frit [12]. The thickness of the inlet and outlet frits is 0.81 mm, their total length accounting therefore for 1.6% of the column length. Their relative contribution to radial dispersion can be considered as negligible. The modification of the outlet endfitting consisted in drilling a larger open access (4.5 mm I.D.) through the frit retainer. This frit is maintained in its original position and its diameter matches exactly the column tube diameter (4.6 mm I.D.). The height of the frit retainer was shortened by about 4 mm. The screw endfitting bolt was also modified by cutting 10 mm off its top and a 5 mm I.D. hole was drilled to facilitate access of the Micro-electrodes. The diameter of the glass tip of the micro-electrode is about 0.25 mm. The diameter of the encapsulated platinum wire at the tip of the micro-electrode is 25 μm. Accordingly, the position of the micro-electrode in contact with the wall of the opened frit retainer allows to detect the solute at a distance from the column wall no closer than 0.050 (half the difference between the 4.5 mm diameter of the frit retainer and the 4.6 mm diameter of the column) + 0.125 (micro-electrode tip radius) = 0.175 mm corresponding to a reduced radial coordinate of $x = (2.300 - 0.175/2.300) = 0.92$.

3.4. Apparatus

The LED data were acquired with an Agilent 1090 HPLC system (Agilent Technology, Waldbronn, Germany) liquid chromatograph. This instrument includes a ternary pump with solvent selection valves, an auto-sampler with a 25 μL sample loop, a column thermostat, a diode-array UV-detector (1.7 μL, upper sampling rate at 25 Hz), and a Chemstation data software. The maximum flow rate and the upper pressure limit that can be applied are 5.0 mL/min and 400 bar, respectively. The system was optimized by using 120 μm I.D. inlet capillary tubings in order to minimize the extra-column band broadening before the sample enters the column.

The flow rate accuracy was checked at ambient temperature by directly collecting the mobile phase in the absence of column at 295 K and at flow rates of 0.1, 1, and 2.5 mL/min during 50, 25, and 10 min, respectively. The relative errors were all always less than 0.4%, so we estimate the long-term accuracy of the flow rate at 4 μL/min or better at flow rates around 1 mL/min. The laboratory temperature was controlled by an air conditioning system set at 295 K. The daily variation of the ambient temperature never exceeded ±1 °C.

One working micro-electrode was positioned at the center of the outlet frit (r = 0.00 mm). The second was laterally in contact with the wall of the frit retainer previously drilled (r = 2.12 mm). During all the series of experiments, the two working micro-electrodes were maintained in their original position. The counter electrode was a platinum wire in contact with the solution exiting the column. The reference electrode was made of Ag/AgCl in a saturated aqueous solution of potassium chloride (>3 M). The concentration of KCl in the mobile phase was fixed at 50 mM. The four electrodes were connected to a scanning electrochemical microscope (CH instruments, Austin, TX, USA) used for measuring the currents at constant potential. Para-benzoquinone and fructose were detected at constant potentials of 0.7 and 0.9 V, respectively, *versus* Ag/AgCl.

The HETP data were acquired with the Agilent 1290 Infinity system (Agilent Technology, Waldbronn, Germany). This chromatograph includes a 1290 Infinity binary pump with solvent selection valves and a programmable auto-sampler. The injection volume was set at 0.2 μL. The instrument is equipped with a two-compartment oven and a multi-diode-array UV–VIS detection system. The temperature of the detection cell is automatically kept at 313 K. The system is controlled by the Chemstation software. The sample trajectory in the equipment involves passage through

- A 20 μL injection loop attached to the injection needle.
- A small volume needle seat capillary (red tubing), ≃1.7 μL, between the injection needle and the injection valve. The total volume of the grooves and connection ports in the valve is around 1.2 μL.
- Two connector capillaries (red tubing), both with 85 μm I.D. and 250 mm long, one before the column and after the injection valve and the second between the column and the detector cell. Their total volume is 2.8 μL.
- A small volume detector cell, 0.8 μL.
- The signal is acquired with a sampling rate of 80 Hz.

The total extra-column volume is then close to 6.5 μL and the half-height peak variance around 3.0 μL^2 at a flow rate of 1 mL/min.

4. Results and discussion

In a first part, we measured simultaneously the elution times of para-benzoquinone at the wall and at the center of the outlet frit of the 100 × 4.6 mm 2.5 μm Kinetex-C_{18} packed column 1. Three different retention factors (k' = 0.1, 0.7, and 3.0) were chosen by adjusting the methanol content in the aqueous mobile phase (70%, 35%, and 10% methanol, respectively). For each retention factor, a series of 5 different flow rates was applied. Each measurement was repeated six time, therefore a total of 2 (wall and center locations) × 3 (retention factors) × 5 (flow rates) × 6 (repeats) = 180 amperograms were recorded. During all this series of experiments, the positions of the two micro-electrodes in contact with the outlet frit were not changed. Note that the intensity recorded with the micro-electrode placed at the wall was systematically larger than that measured with the second micro-electrode, placed at the center of the column. Switching the positions of these two micro-electrodes, however, generated a higher signal at the column center showing that the difference in intensity was related to a difference in the response of the two micro-electrodes. The actual reason for this effect (different electrode surface area, degree of polishing, activation, etc.) was not investigated in this work.

In a second part, we compared the LED observations and measurements of the relaxation rate of the radial concentration gradients caused by the trans-column flow heterogeneity.

In the third part of this work, we report on records of HETP data for four compounds (uracil, acetophenone, toluene, and naphthalene) with retention factors between 0 and 3 on the second Kinetex-C_{18} column. LED measurements were also performed with this column afterward. We finally conclude on the impact of retention on the trans-column eddy diffusion term and on the performance of RPLC columns.

4.1. Local electrochemical detection

In the following sections, the experimental parameter $\omega_{\beta,c}$ is the relative difference between the elution times of the peak apices of the solute measured at the center (t_{center}) and the wall (t_{wall}) of the column:

$$\omega_{\beta,c} = \frac{t_{wall} - t_{center}}{t_{center}} \quad (22)$$

We call it the apparent relative velocity bias. In slurry-packed beds, the local flow velocity is smaller along the column wall than in its center. The opposite is true for monolithic columns. Measurements of the apparent relative velocity bias were made for the same compound, para-benzoquinone, eluted with an eluent of different composition, giving three different retention factors.

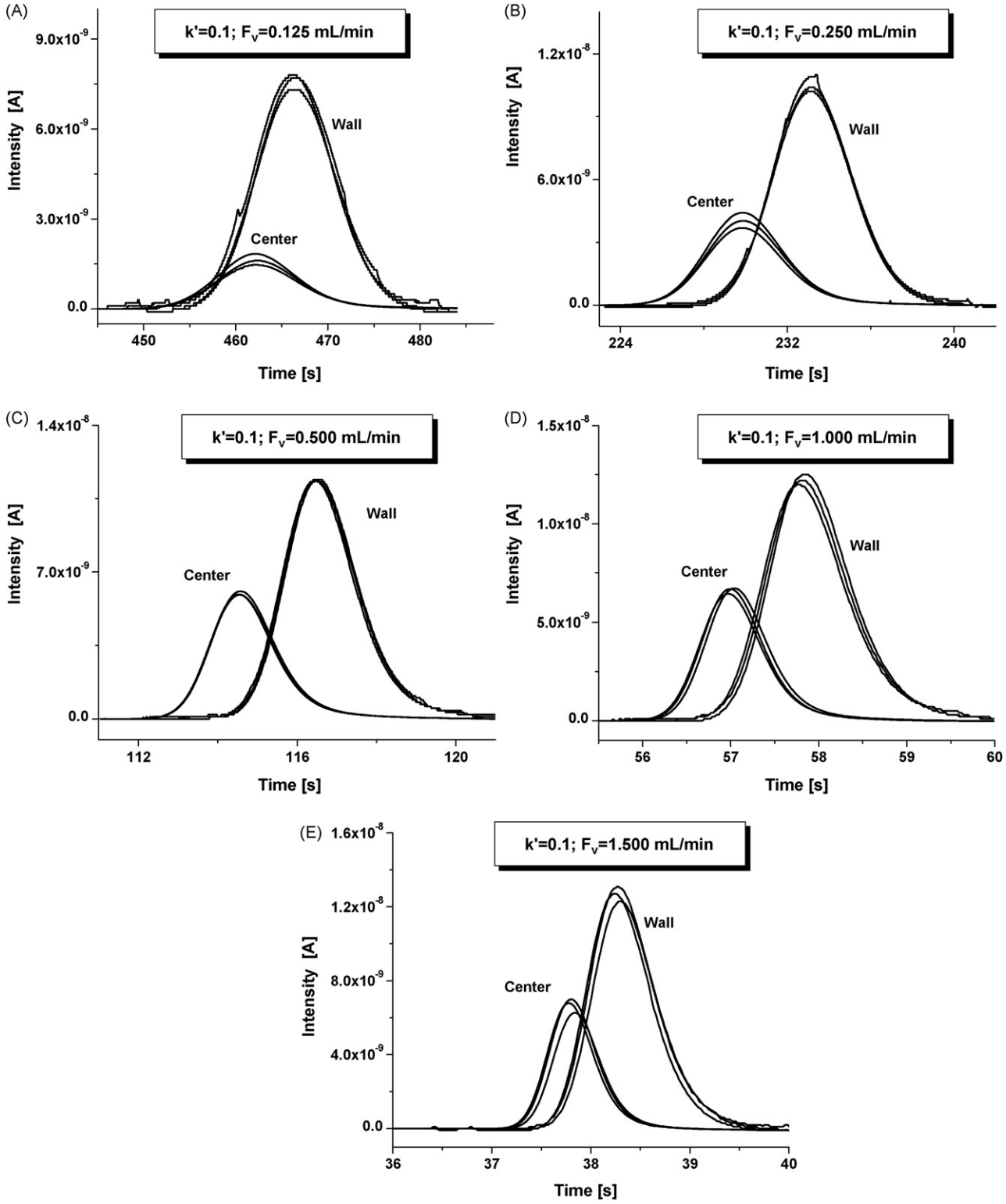

Fig. 1. Amperograms of para-benzoquinone recorded simultaneously with two micro-electrodes located at the center ($r = 0$) and close to the edge ($r = 2.13$ mm) of the outlet frit of column 1 (4.6 mm × 100 mm, packed with 2.5 μm shell particles). The potential of these two working electrodes was set constant at + 0.7 V with respect to the reference potential (Ag/AgCl). The mobile phase was a mixture of methanol and water (70/30, v/v) giving for the retention factor of para-benzoquinone $k' = 0.1$. The temperature was 294 ± 1 K. Five different flow rates were applied, 0.125 (A), 0.250 (B), 0.500 (C), 1.000 (D) and 1.500 mL/min (E). At each flow rate, six replicate measurements were carried out (for the sake of clarity, three records only are shown in the graph).

4.1.1. Quasi-unretained compounds, k′ < 0.1

The methanol concentration of the aqueous mobile phase (50 mM KCl) was set at 70%. Based on pycnometric measurements, the hold-up volume of the 100 × 4.6 mm Kinetex column was estimated at 0.88 cm^3 (total porosity $\varepsilon_t = 0.53$). The retention factor of para-benzoquinone is close to 0.1. Fig. 1A–E shows the corresponding amperograms recorded at flow rates of 0.125 (A), 0.250 (B), 0.50 (C), 1.00 (D), and 1.50 (E) mL/min. The relative difference of average

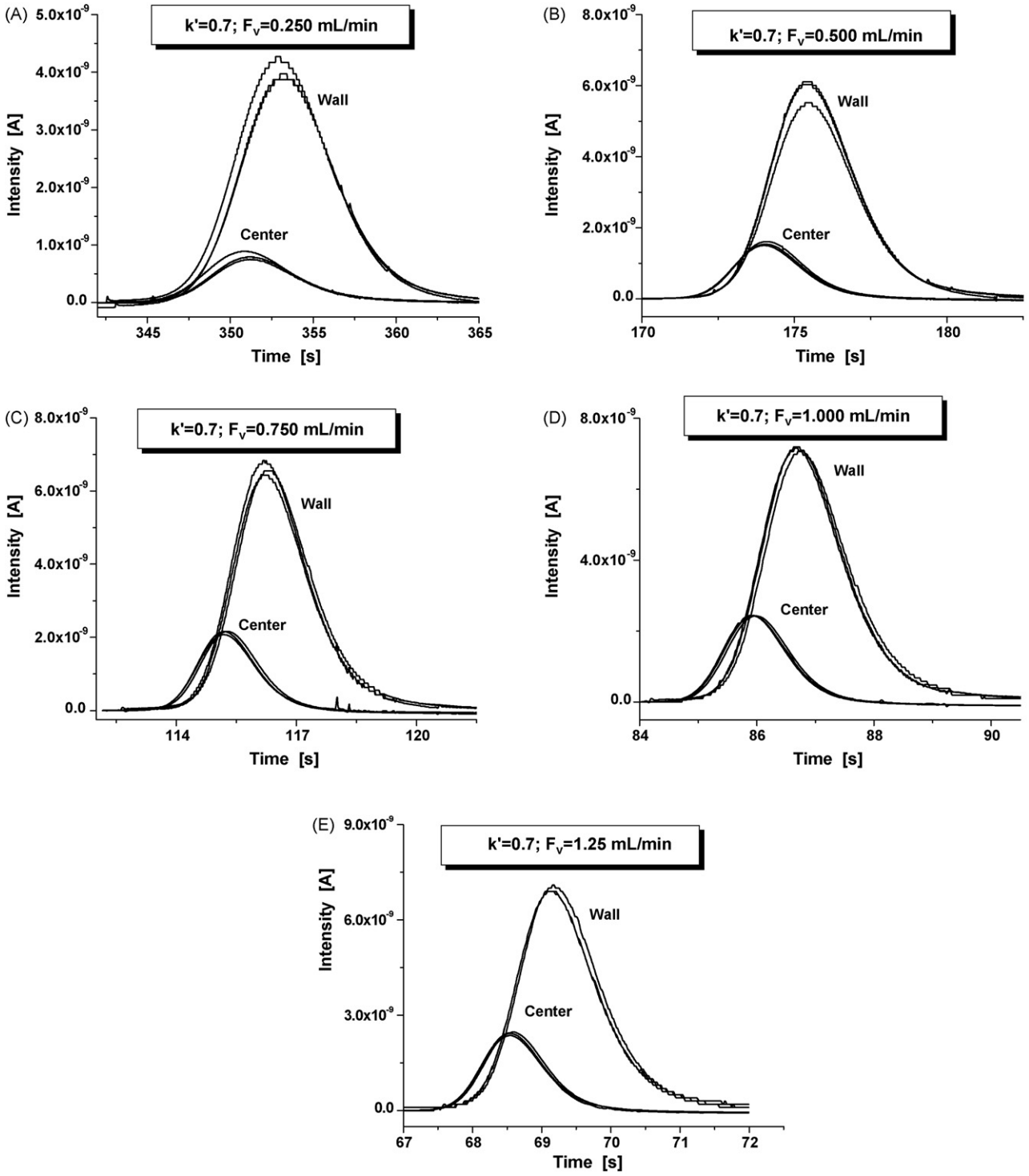

Fig. 2. Same as in Fig. 1, except the volume fraction of methanol was decreased to 35% so $k' = 0.7$ and the flow rates were: 0.25 (A), 0.50 (B), 0.75 (C), 1.00 (D), and 1.25 mL/min (E). Note the decrease of the relative difference between the elution times measured at the wall and at the center of the outlet frit compared to the values in Fig. 1.

linear velocities of the sample zone between the center and the wall of the column are equal to 0.90%, 1.44%, 1.68%, 1.43%, and 1.20%, respectively (Fig. 4). This difference increases first with increasing flow rate, reaches a maximum at about 0.50 mL/min, and eventually decreases with further increase of the flow rate, up to 1.5 mL/min.

These experiments demonstrate that the trans-column eddy diffusion term and the relaxation of the radial concentration gradient in packed beds depend on the flow rate for two reasons: (i) the radial dispersion coefficient increases (Eq. (7)) and (ii) the time spent by the sample molecules inside the column decreases with increasing flow rate.

4.1.2. *Weakly retained compounds, $0.5 > k' < 1$*

The methanol concentration was decreased from 70% to 35% while keeping constant the concentration of potassium chloride in the mobile phase (50 mM KCl). The retention factor of parabenzoquinone increased from 0.1 to 0.7. Five different flow rates were successively applied.

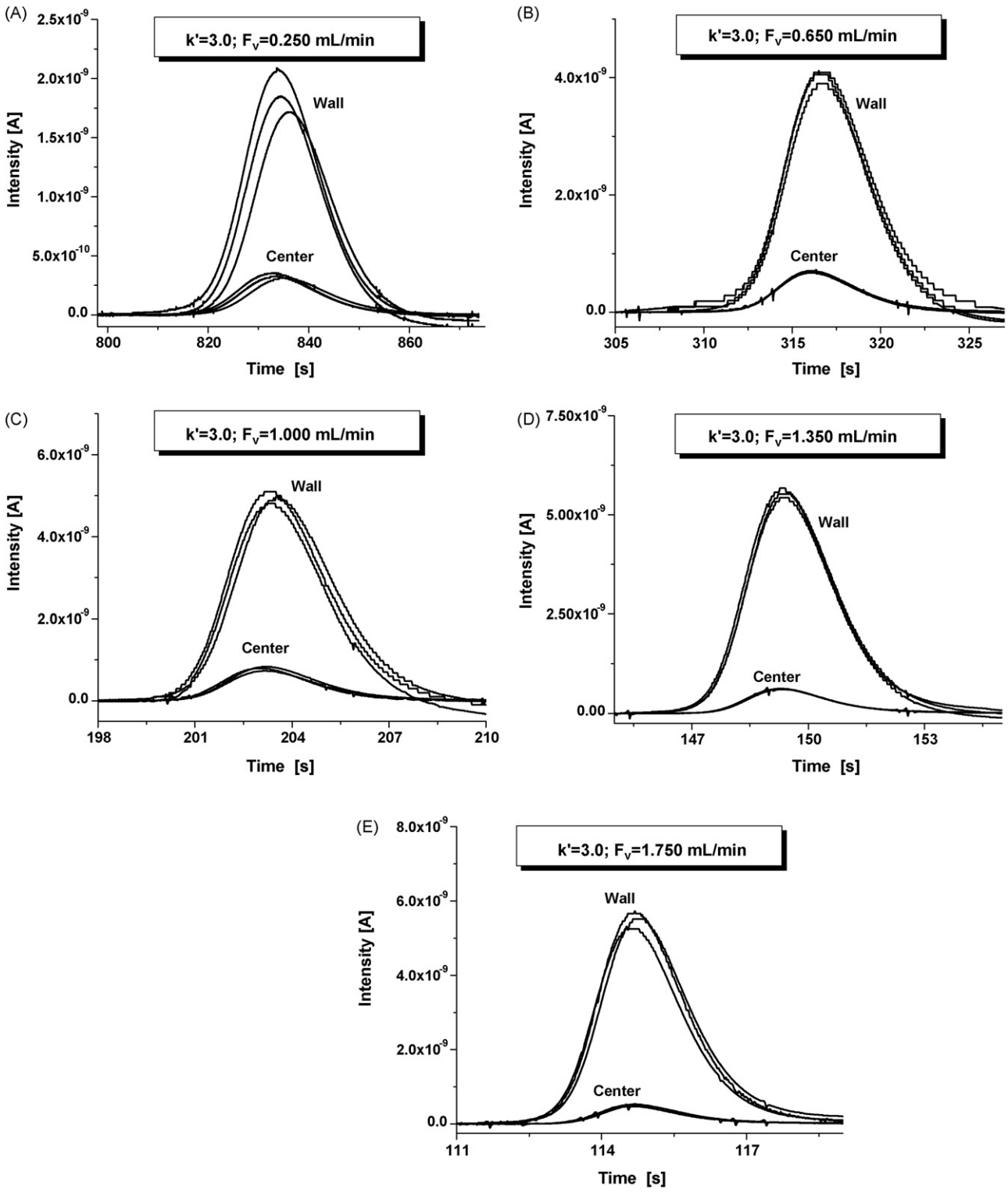

Fig. 3. Same as in Fig. 1, except the volume fraction of methanol was decreased to 10% so k' = 3.0 and the flow rates were: 0.25 (A), 0.65 (B), 1.00 (C), 1.35 (D), and 1.75 mL/min (E). Note the nearly identical elution times at the wall and at the center of the column outlet.

Fig. 2A–E shows the corresponding amperograms. The average retention times of the elution zone was measured and the relative difference of average linear velocities of the solute between the center and the wall of the column were found to be 0.59%, 0.80%, 0.88%, 0.87%, and 0.84% at the flow rates of 0.25, 0.65, 1.00, 1.35, and 1.75 mL/min, respectively (see Fig. 4B). Strikingly, the moderate increase of the retention factor of the solute has a significant impact on the apparent trans-column velocity biases observed. These biases are about half as large as they are for a retention factor of 0.1. This decrease of the apparent trans-column velocity biases is not mainly due to the larger time spent by the molecule in the column: in Figs. 1C and 2C the residence time in the column was the same, yet the difference in $\omega_{\beta,c}$ values is significantly smaller, only equal to 0.8%. This difference is accounted for by the increase of the

Table 2
Calculated values of D_0 (Eq. (7)), D_r (Eq. (7)), and A_0 (Eq. (11)).

k'	$10^6 \times D_0$ [cm^2/s]	F_v [cm^3/min]	$10^6 \times D_r$ [cm^2/s]	$10^7 \times A_0$
0.1	4.63	0.125	5.89	3.16
		0.250	7.15	2.55
		0.500	9.66	1.83
		1.000	14.7	1.17
		1.500	19.7	0.86
0.7	4.03	0.250	6.54	2.33
		0.500	9.05	1.60
		0.750	11.6	1.22
		1.000	14.1	0.99
		1.250	16.6	0.83
3.0	2.91	0.250	5.42	1.87
		0.650	7.94	1.00
		1.000	13.0	0.70
		1.350	16.5	0.55
		1.750	20.5	0.43

radial dispersion coefficient with increasing flow rate (0.50 mL/min in Fig. 1C *versus* 0.75 mL/min in Fig. 2C). Table 2 lists the values calculated for $\overline{D_r}$ according to Eq. (7). Lower trans-column relative velocity biases are expected when the retention factor of the solute increases further.

4.1.3. Retained compounds, $k' > 3$

The retention factor of para-benzoquinone was finally raised to 3.0 by decreasing the volume fraction of methanol to 10%. The flow rates were set at 0.25, 0.65, 1.00, 1.35, and 1.75 mL/min. The experimental band profiles are shown in Fig. 3A–E. The results are striking. Even for this moderate retention factor, the relative differences between the elution times of the solute zone at the wall and at the center never exceed 0.16%. In other words, the actual heterogeneity of the flow velocities in a packed column that is easily measured with a non-retained compound becomes barely detectable with a retained compound. This observation is of paramount importance because it provides the fundamental explanation for the greater efficiency exhibited by RPLC columns for strongly retained compounds. Fig. 4C summarizes the experimental and apparent trans-column velocity biases for flow rates in the range between 0.25 and 1.75 mL/min. As for retention factors of 0.1 and 0.7, the trans-column migration velocity biases increase first (because the time spent in the column is decreasing), then decrease (because the radial dispersion coefficient increases). The amplitude of these variations, however, remains extremely small.

Figs. 3E, 2C, and 1C illustrate the fact that, at a constant elution time (t_R = 115 s), the difference between the first moments measured at the column outlet wall and in its center is accounted for by the radial dispersion coefficient increasing with increasing flow rate. We measured $\overline{D_r} = 9.6 \times 10^{-6}$, 11.6×10^{-6}, and 20.5×10^{-6} cm^2/s at the flow rates of 0.50, 0.75, and 1.75 mL/min, respectively. Accordingly, the relative apparent velocity biases decrease from to 1.68% to 0.88% and 0.02% for k' = 0.1 (0.50 mL/nim), 0.7 (0.75 mL/min), and 3.0 (1.75 mL/min), respectively.

4.2. Interpretation of the facts

This series of local detection measurements shows that the retention times of solutes eluted from packed columns and the mobile phase flow rates have a significant impact on the trans-column eddy diffusion term. The experimental results show that the important diminution of the apparent trans-column velocity biases that is observed results from an increase of either the retention time, t_R, or the radial dispersion coefficient, $\overline{D_r}$. On the basis of this result, we propose a simple physical model that can explain these observations.

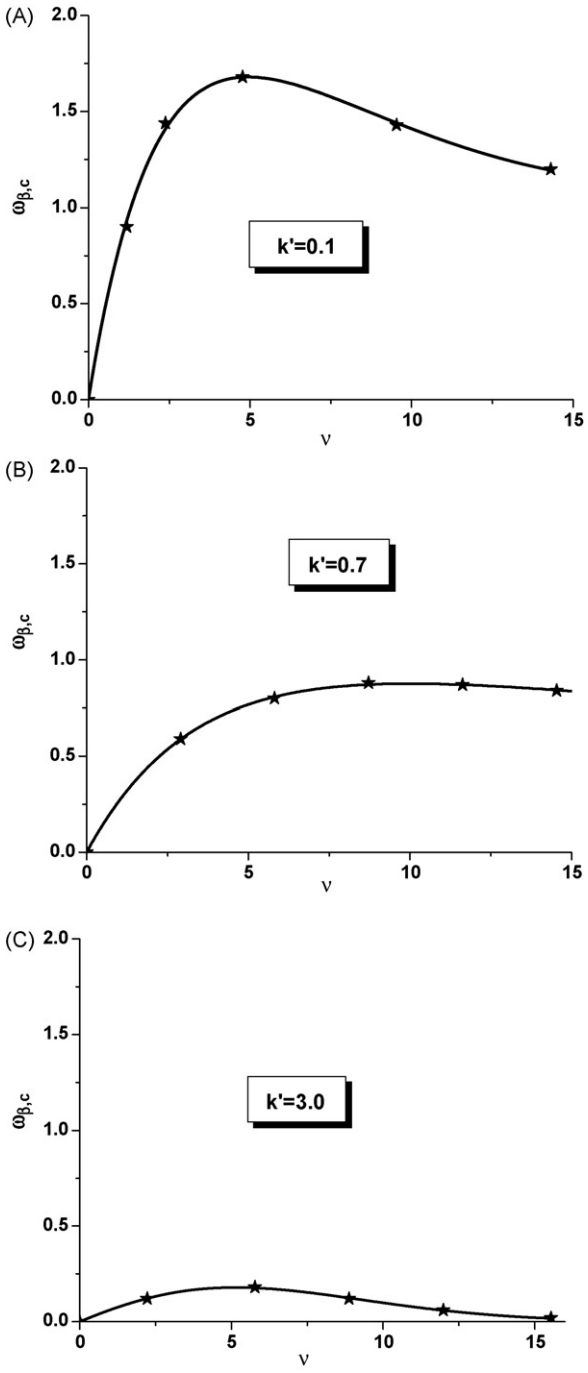

Fig. 4. Plot of the experimental apparent velocity biases, $\omega_{\beta,c}$, of para-benzoquinone as a function of the reduced interstitial linear velocity for three values of the retention factors, k' = 0.1 (A), k' = 0.7 (B), and k' = 3.0 (C). Note the continuous decrease of the velocity biases with increasing retention factor. Same column as in Fig. 1.

4.2.1. A qualitative physical model

In this section, we assume that the inlet frit is ideal, i.e., that the distribution of the sample concentration across the column diameter at column inlet z = 0 is uniform. We also assume that the flow profile across the cylindrical packed bed is radially heterogeneous, a direct consequence of the slurry packing process and of the radial variation of the shear stress applied to the bed during its packing [6]. Because the shear stress is smaller in the column center than along

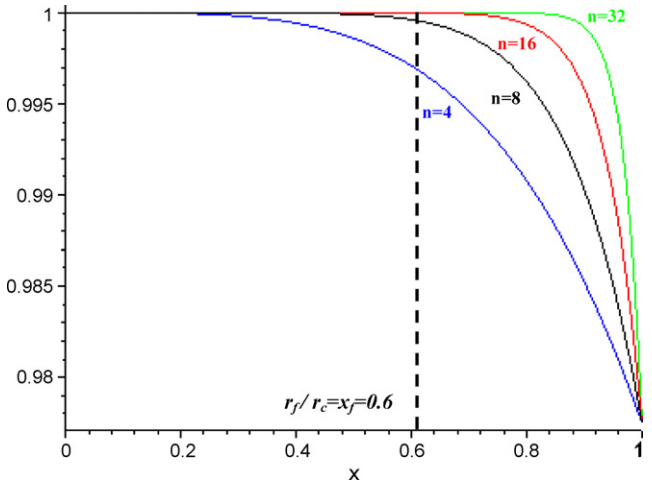

Fig. 5. Examples of normalized radial flow velocity distributions, $u(x)/u(0)$, according to the polynomial Eq. (2) ($\omega_{\beta,c}$ = 2.25%) for n = 4, 8, 16, and 32. The parameter n determines the extent of uniformity of the flow distribution in the center region of the column cross-section. The vertical dashed line locates the critical radius above which the linear velocity is heterogeneous in the column used 1 ($n \simeq 12$).

its wall, the external porosity is locally larger in the center than at the wall. Accordingly, the local flow rate is faster in the central region than near the wall, consistent with the observations shown in Figs. 1, 2, and 3. Eq. (2) describes reasonably well the radial velocity profile across the column [11]. In this equation, the parameter n allows a definition of a critical reduced radius, x_f, below which the flow velocity remains practically uniform. For instance, Fig. 5 illustrate that x_f = 0.20, 0.48, 0.70, and 0.84 for n = 4, 8, 16, and 32, respectively.

The combination of a trans-column flow heterogeneity becoming important in the wall region and of a radial dispersion of the solute concentration is consistent with the observations made at constant k'. On the one hand, at low flow rates, the apparent velocity biases are small and increase because only molecular diffusion (D_0) across the bed effectively contributes to relax radial concentration gradients. On the other hand, at high flow rates, the apparent velocity biases decrease with increasing flow rate because transverse eddy diffusion, D_{eddy}, helps to mix the sample across the column. Eventually, a maximum radial heterogeneity is observed for an intermediate flow rate, between 0.5 and 1.0 mL/min in the case of small molecules. In other words, the true center-to-wall relative velocity biases, $\omega^*_{\beta,c}$, is at least equal to 1.7% because LED data can only approach this parameter from below. This value is consistent with those previously observed in liquid chromatography ($\simeq$2%), in studies made using similar techniques of heterogeneity measurements at the column outlet [11,12].

The radial dispersion coefficient across a packed column can be estimated from the combination of the results of peak parking measurements (static diffusion coefficient, D_0) and of NMR experiments (contribution of eddies to transverse dispersion, γ_r). Accordingly (see Eq. (7)), the radial dispersion coefficients, $\bar{D}_r$, of benzoquinone at a flow rate of 1.00 mL/min and for retention factors of 0.1 and 3.0 are equal to 1.47×10^{-5} and 1.30×10^{-5} cm^2/s, respectively. Based on the experimental data in Figs. 1D and 3C, the elution times t_R are equal to 58 and 204 s. Therefore, according to Eintein's law of diffusion in a cylindrical tube ($(\delta r)^2 = 4D_r t_R$), the radial displacements, δr, of the molecules are equal to 0.58 and 1.03 mm, respectively. This distance is clearly shorter than the column radius (2.3 mm) suggesting that the sample cannot statistically sample the column radius during elution.

In order for the molecules of a solute to statistically sample the whole column diameter during its elution, the following condition should be verified:

$$\frac{4\overline{D_r}t_R}{r_c^2} \geq 1 \tag{23}$$

At all flow rates between 0.25 and 1.75 mL/min and for k' = 3, the dimensionless quantity in Eq. (23) is no larger than 0.34. It never exceeds 0.05 for k' = 0.1 nor for k' = 0.7. Obviously, solute molecules cannot statistically sample the whole column cross-section under such experimental conditions even when the solute is retained. Yet, Fig. 4A–C demonstrates experimentally that the quantity $\omega_{\beta,c}$ drops from about 1.5% to nearly zero when the retention factor increases from 0.1 to 3.0. It would erroneously appear to the analyst that the solute molecules have sampled the whole column radius.

Most likely, the flow heterogeneity is pronounced only in the region close to the column wall. The platinum tips of the Microelectrodes are located at about 0.175 mm from the column wall or only 92% of the column radius, r_c. Although we do not measure the elution band profile at the very wall of the column, velocity biases were unambiguously measured under non-retained conditions, i.e., at $x_f < 0.9$.

Let us assume a uniform flow profile (no velocity biases) in the center region of the column up to the critical reduced radius, x_f. The characteristic diffusion length in Eq. (23) over which radial concentration gradients exist would then reduce to $r_c(1 - x_f)$ because the flow heterogeneity is virtually zero between x = 0 and $x = x_f$. At the highest flow rate applied ($\simeq$1.75 mL/min) and for the largest retention factor, the quantity in Eq. (23) is larger than unity if $x_f > 0.6$. This suggests that the local external porosity begins to drop beyond a distance of *ca.* 60% of the column radius. This agrees well with the void fraction profile calculated across the column after consolidation of the bed [6]. Accordingly, the transverse velocity biases at the column outlet can be measured only if the average displacement of the sample molecules exceeds 0.9 mm. Substituting this value as the new characteristic diffusion length in Eq. (23), we obtained values of 0.32, 0.48, and 1.00 for k' = 0.1 (1.5 mL/min), k' = 0.7 (1.25 mL/min), and k' = 3.0 (1.75 mL/min), respectively. This is consistent with the decrease of the apparent velocity bias when the retention factor increases from 0.1 to 3.0. Fig. 6A shows the correlation between the values of $\omega_{\beta,c}$ and $4\overline{D_r}t_R/[r_c(1 - x_f)]^2$ within the range of flow rates in which the transverse eddy diffusion contribution exceeds 60% of the radial dispersion coefficient. The dotted lines were drawn only to guide the eye of the reader and make it easier to appreciate the correlation between the relative velocity bias and the normalized variance of the radial displacement. Fig. 6B shows the same correlation but within the range of low velocities in which the contribution of eddy diffusion to radial dispersion is smaller than 50%. The correlation is less tight than at high flow rates, suggesting that the variation of the radial dispersion coefficient with k' derived from Eq. (7) is only approximate. Yet, increasing the flow rate at constant retention factor is always accompanied by an increase of the apparent velocity biases, $\omega_{\beta,c}$, because the time spent inside the column decreases.

From the extrapolation of the plot in Fig. 5B at low flow rates and small retention factors, it is possible to approach the true and physically correct flow velocity bias, $\omega^*_{\beta,c}$, between the wall and the center of the column. It is approximately equal to about 2.25%.

4.2.2. A quantitative model for trans-column eddy diffusion in packed beds

In the previous section, we concluded that the radial distance over which radial flow heterogeneity persists across the column is significantly shorter than the column radius. Flow heterogeneities are essentially located between r_f = 1.4 and r_c = 2.3 mm. Consequently, the radial concentration gradients are eventually relaxed when the radial displacement of the solute molecules during their

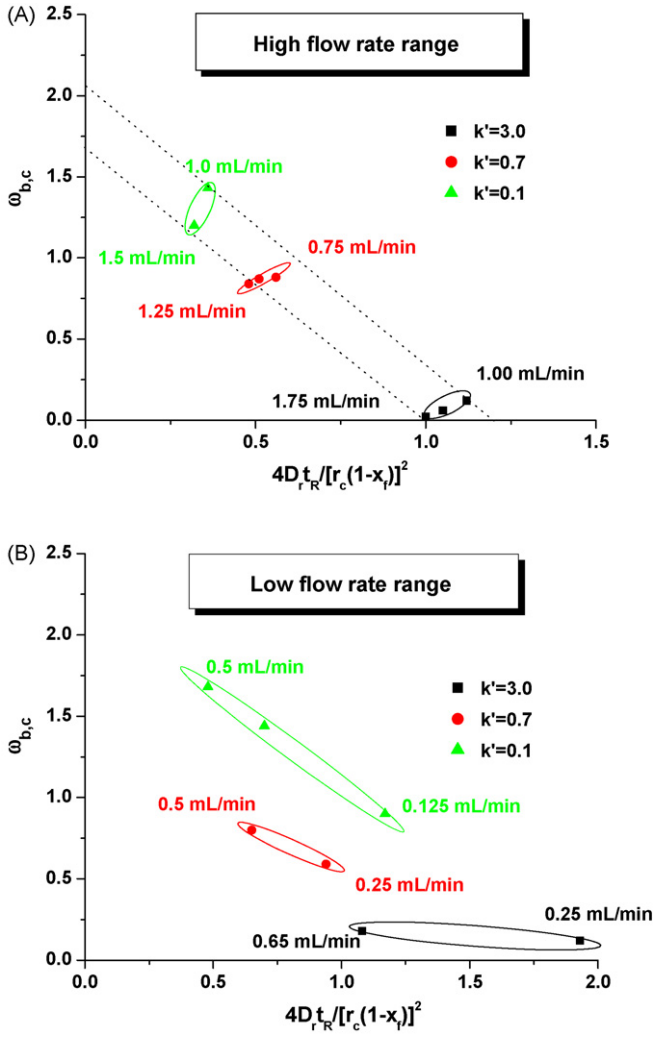

Fig. 6. Plots of the experimental (LED) apparent relative velocity bias, $\omega_{\beta,c}$, as a function of the ratio of the radial displacement variance $4D_r t_R$ (representing the average displacement squared of the sample molecules during their migration along the column) to the radial distance squared $r_c(1-x_f)$ (representing the characteristic distance squared of flow heterogeneity in the column). Same column as in Fig. 1. (A) High flow rate range. Note the good correlation between the three groups of data points (three retention factors 0.1, 0.7, and 3.0) and the velocity bias measured at high flow rates. (B) Low flow rate range. The smaller the retention factor, the faster the velocity biases increases with increasing flow rate.

elution is about 0.9 mm, a distance shorter than the column radius. Fig. 5 represents different normalized flow profiles for different values of the parameter n, according to Eq. (2). The experimental data are consistent with $n = 12$, for which the local flow rate remains uniform from $x = 0$ to about $x = 0.6$.

If radial dispersion is strictly equal to zero, the eddy diffusion term expected for small relative velocity biases, $\omega^*_{\beta,c}$, is independent on the flow rate and is given by Eq. (19). When the compound has enough time to statistically sample the whole column diameter, which depends on the retention time, t_R, and the radial dispersion coefficient, D_r, the conditions of Aris are satisfied and the eddy diffusion term is directly proportional to the velocity of the compound [14,15]. The corresponding reduced HETP is given by Eq. (9).

According to the coupling theory of Giddings, the general eddy diffusion term can be written according to Eq. (21). The values of A_0 (Eq. (11)) and D_0 (Eq. (7)) are listed in Table 2 for all flow rates and retention factors applied in this work. Fig. 7 shows the reduced eddy diffusion term of para-benzoquinone caused by the sole trans-column effect for the three retention factors applied in this work.

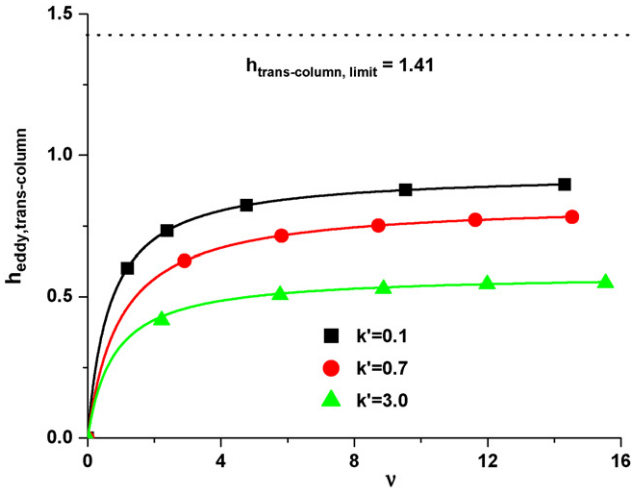

Fig. 7. Plot of the theoretical trans-column eddy diffusion term of para-benzoquinone according to Eq. (21) based on the experimental determination of $\omega_{\beta,c} = 2.25\%$ and $n = 12$ by LED detection. Same column as in Fig. 1. Note the predicted impact of k' on the trans-column eddy diffusion term of para-benzoquinone. The horizontal dashed line represents the theoretical limit of the trans-column eddy diffusion term in the absence of radial dispersion.

The most interesting observation is that the trans-column eddy diffusion term clearly depends on the retention factor of the compound. At a reduced linear velocity of 8, this reduced eddy diffusion terms are 0.87, 0.74, and 0.52 for $k' = 0.1$, 0.7, and 3.0, respectively.

In the next section, we validate this observation by discussing the reduced HETP of four independent compounds having retention factors between 0 and 3.0 on the Kinetex-C_{18} column 2.

4.3. Relationship between trans-column velocity biases and chromatographic kinetic performance: HETP data

Fig. 8 shows the reduced HETP plots in logarithm scale of uracil (full black squares), acetophenone (full red circles), toluene (full green upward triangles), and naphthalene (full blue downward triangles). The average particle size is 2.5 μm, according to the mean

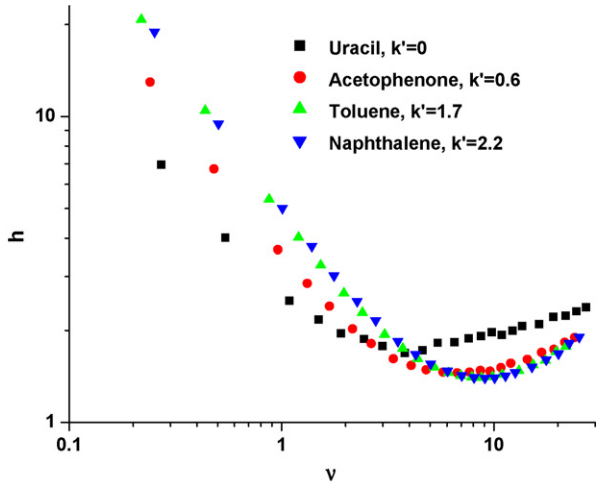

Fig. 8. Plot of the reduced HETPs (log h) for uracil (full black squares), acetophenone (full red circles), toluene (full upward green triangles), and naphthalene (full blue downward triangles) measured with column 2. Eluent: mixture of acetonitrile and water (65/35, v/v). Temperature: 294 ± 1 K. Flow rate range: 0.04–4.00 mL/min (two decades). Note how the minimum HETP decreases and the optimum flow velocity increases with increasing retention factor of the small molecules. (For interpretation of the references to colour in this figure legend, the reader is referred to the web version of the article.)

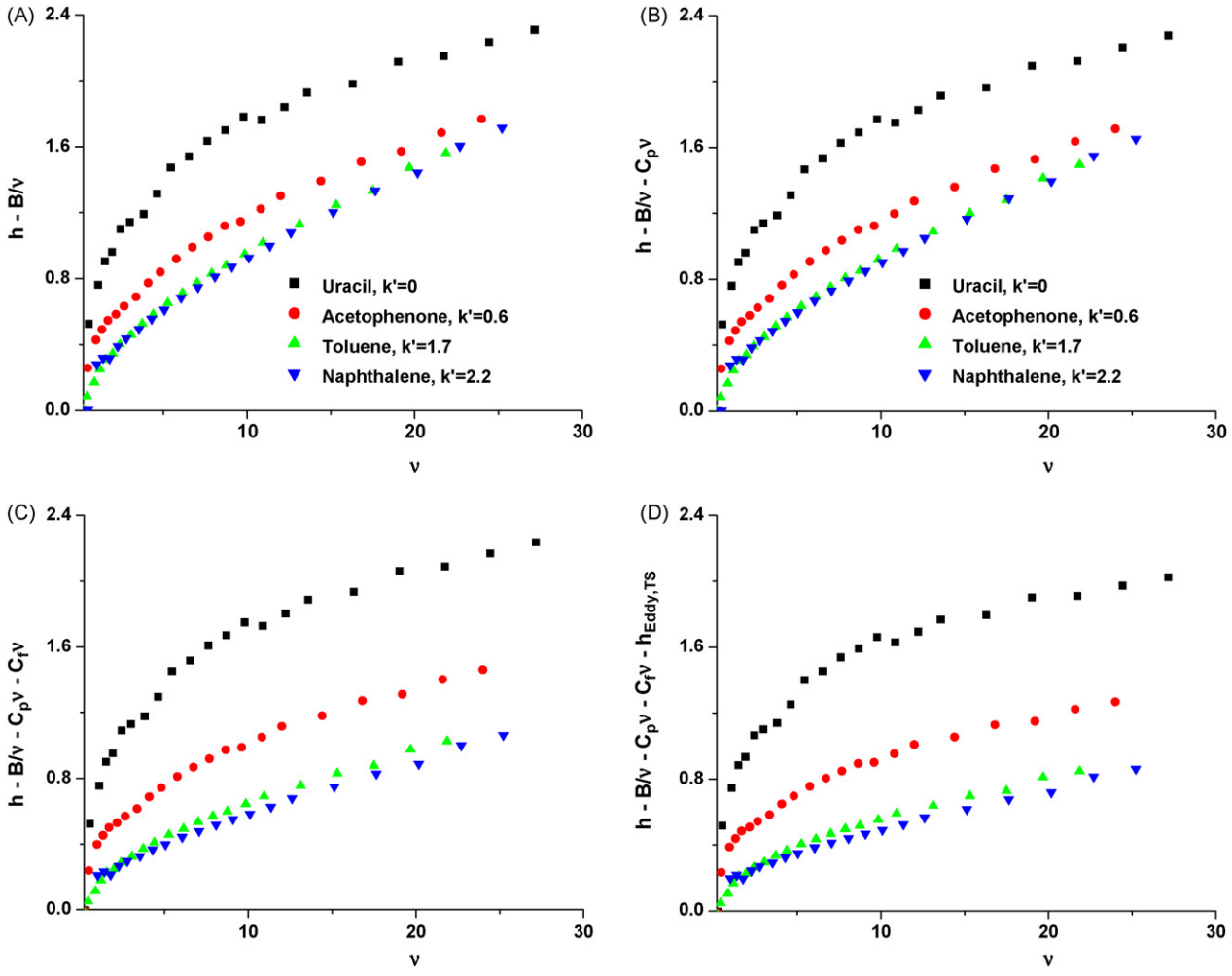

Fig. 9. Successive corrections of the reduced HETP by subtractions of the longitudinal diffusion term B/ν (A), the solid–liquid trans-particle mass transfer resistance term $C_p\nu$ (B), the solid–liquid external film mass transfer resistance term $C_f\nu$ (C), and the short-range inter-channel eddy term $h_{Eddy,TS}$ (D), from the experimental reduced HETP, h. Column 2. The residual data plots in (D) represent the sums of only the contributions of the short-range inter-channel and the trans-column eddy diffusion terms.

particle size measured with a Coulter counter [13]. The mobile phase was a mixture of acetonitrile and water (65/35, v/v) and the temperature was ambient (294 ± 1 K). The bulk molecular diffusion coefficients, D_m, of acetophenone, toluene, and naphthalene, were estimated from the extension of the Wilke and Chang equation in pure eluents [20] to binary mixtures of eluents [21]. They are equal to 1.03×10^{-5}, 1.14×10^{-5}, and 9.87×10^{-6} cm^2/s, respectively. The diffusion coefficient of uracil was obtained from Ref. [22] after correction for the mobile phase viscosity taken from reference [23]. It was estimated at 9.10×10^{-6} cm^2/s. The HETP data were all corrected for the extra-column contributions. Fig. 8 shows that the minimum reduced HETP decreases with increasing retention factor, from 1.69 to 1.46, 1.40, and 1.39 for k' = 0, 0.6, 1.7, and 2.2, respectively. This decrease is most probably caused by a difference in the A term of the HETP plots of these compounds. So, we isolated the contributions of the total eddy diffusion term inside the column by subtracting the contributions of longitudinal diffusion (B term), of the trans-particle mass transfer (C_p term), and of the external film mass transfer (C_f term).

4.3.1. Longitudinal diffusion B term

The reduced longitudinal term, h_{Long}, is written [5]:

$$h_{Long.} = \frac{B}{\nu} \tag{24}$$

The coefficient B was estimated from the experimental HETP data recorded at the smallest flow rate, F_v = 0.04 mL/min. At this flow rate, the reduced linear velocity is of the order of 0.25 so we can reasonably neglect the contributions of eddy diffusion and solid–liquid mass transfer resistance. Accordingly, B = 1.89, 3.11, 4.53, and 4.78 for uracil, acetophenone, toluene, and naphthalene, respectively. The increase of B with increasing solute retention is consistent with the contribution of internal diffusion through the porous shell of the Kinetex-C_{18} particles. This method is validated by the comparison of the B coefficients thus obtained and those measured by the peak parking method (see next section), which are 1.82, 2.97, 4.42, and 4.57, respectively, values that are less than 5% smaller than the previous ones. The plots of $h - (B/\nu)$ *versus* ν are shown in Fig. 9A. These plots show that the eddy diffusion terms of compounds tend to decrease with their increasing retention because diffusion coefficients and retention factors in RPLC tend to be inversely correlated.

4.3.2. Trans-particle mass transfer resistance C_p term

The following general expression for the C_P term of shell particles was recently derived from a theoretical point of view [24]:

$$C_p = \frac{1}{30}\frac{\varepsilon_e}{1-\varepsilon_e}\left[\frac{k_1}{1+k_1}\right]^2 \frac{1+2\rho+3\rho^2-\rho^3-5\rho^4}{(1+\rho+\rho^2)^2}\frac{1}{\Omega} \tag{25}$$

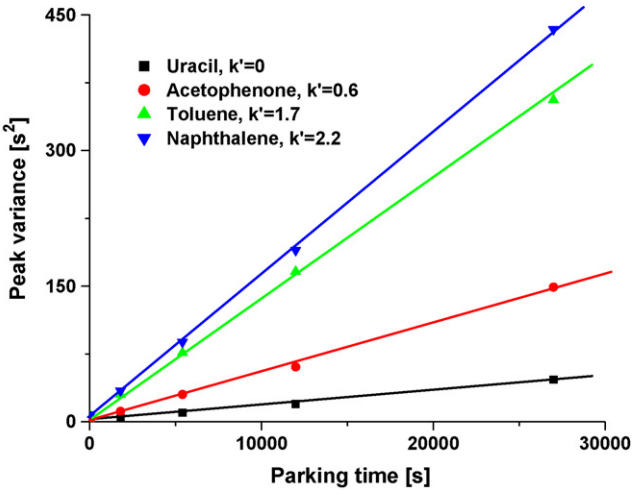

Fig. 10. Results of peak parking measurements, plots of the elution peak variance as a function of the parking time, t_p. The flow rate was fixed at 0.44 mL/min. The temperature was 294 ± 1 K. Column 2.

where

$$k_1 = \frac{1-\varepsilon_e}{\varepsilon_e}[\varepsilon_{shell,p} + (1-\varepsilon_{shell,p})K_{shell}](1-\rho^3)$$

where K_{shell} is the Henry constant for the adsorption–desorption equilibrium of the solute in the porous shell adsorbent. It is derived from the experimental retention factor k':

$$K_{shell} = \frac{\varepsilon_t k'}{(1-\varepsilon_e)(1-\rho^3)(1-\varepsilon_{p,shell})} \quad (27)$$

In Eq. (25), the parameter Ω was derived from the results of peak parking experiments, as described in detail in Ref. [13]. Fig. 10 shows plots of the total variance of the bands of uracil, acetophenone, toluene, and naphthalene as functions of the parking time, t_p, inside the column (t_p = 1, 30, 90, 200, and 450 min). The bands were eluted at the constant flow rate of 0.44 mL/min, with the same mobile phase as that used to measure the HETPs. Assuming a parallel model for the diffusion in and out of the particle, the determination of the parameter Ω is straightforward [1,2,13]. Values of 0.34, 1.05, 1.57, and 2.01 were obtained for uracil, acetophenone, toluene, and naphthalene, respectively, giving for k_1 corresponding values of 0.24, 0.99, 2.35, and 2.98, respectively. Fig. 9B shows the plots of $h-(B/\nu)-C_p\nu$ as functions of ν. The difference between Fig. 9A and B shows clearly that the trans-particle mass transfer resistance term is negligible compared to the eddy diffusion and external film mass transfer resistance terms.

4.3.3. External film mass transfer resistance term, C_f

The validity of derivations of the C_f coefficient from the Wilson and Geankoplis correlation [25] was recently validated for large non-porous [26] and porous [27] spherical particles. Accordingly, the dimensionless Sherwood number, Sh, which depends on the film mass transfer coeffcient, k_f (cm/s), the particle diameter, d_p (cm), and the bulk molecular diffusion coefficient, D_m (cm²/s) is written [25]:

$$Sh = \frac{k_f d_p}{D_m} = \frac{1.09}{\varepsilon_e^{2/3}}\nu^{1/3} \quad (28)$$

For spherical particles, the C_f term is then written [23]:

$$C_f = \frac{1}{3}\frac{\varepsilon_e}{1-\varepsilon_e}\left[\frac{k_1}{1+k_1}\right]^2\frac{1}{Sh} \quad (29)$$

Fig. 9C shows the residual contribution of eddy dispersion, $h-(B/\nu)-C_p\nu-C_f\nu$, in the Kinetex column 2 for each compound. The final result is striking. Unambiguously, the eddy dispersion term for the non-retained compound uracil is the largest and these terms decrease regularly with increasing retention factor of the solute. This result is consistent with the independent trans-column velocity bias measurement made in the first part of this work. However, the contributions of trans-channel and short-range inter-channel eddy diffusion should be subtracted in order to isolate the trans-column eddy diffusion term.

4.3.4. Trans-channel and short-range inter-channel eddy diffusion terms

The sole contribution of trans-channel eddy diffusion, $h_{Eddy,TS}$, has never been measured in three-dimensional, dense, consolidated bed made of spherical particles, which are all in contact. This term was estimated by Giddings who assumed that the average "typical" size of these inter-particle channels was about $d_p/3$. Accordingly [5]:

$$h_{Eddy,TS} = \frac{0.01\nu}{1+0.01\nu} \quad (30)$$

Obviously, the exchange of molecules between two streamlines of small velocity, close to the particle external surface, and large velocity, at the center of channels between adjacent particles, are exactly the same whether the compound involved is poorly or strongly retained on the particle surface. Subtracting the trans-channel eddy diffusion term from the reduced HETP shown in Fig. 9C Leads to Fig. 9D. Note that the contribution of trans-channel eddy diffusion is small within the range of reduced linear velocities applied (ν < 25, $h_{Eddy,TS}$ < 0.2).

Finally, the contribution of the short-range inter-channel velocity biases was also subtracted from the reduced HETP data shown in Fig. 9D. The direct measurement of this term is not either possible in 3D consolidated beds of spheres. This term essentially depends on the local arrangement of the packed particles at a scale of a few particle diameters. Giddings suggested the following expression [5]:

$$h_{Eddy,SR-IS} = \frac{0.5\nu}{1+0.5\nu} \quad (31)$$

When subtracting this term from the reduced HETP data in Fig. 9D for the most retained compound, naphthalene, negative h values were obtained. They make no physical sense, meaning that the short-range inter-channel eddy diffusion term must be smaller than was predicted by Giddings. Recently, it was demonstrated that the short-range inter-channel eddy term of columns packed with Kinetex-C_{18} particles is expressed as [13,28]:

$$h_{Eddy,SR-IS} = \frac{0.2\nu}{1+0.5\nu} \quad (32)$$

The final results are shown in Fig. 11. All the terms accounting for longitudinal diffusion, trans-particle mass transfer, external film mass transfer, trans-channel, and short-range inter-channel eddy diffusion, accurately measured, were subtracted. The residual reduced HETP values given in Fig. 11 must represent the contribution of the sole trans-column eddy diffusion term, providing proof that the trans-column effects depend strongly on the retention of solutes, as suggested in the first part of this study, on the basis of the results of local electrochemical detection. At the minimum of their respective HETP curves, the trans-column eddy diffusion terms are 1.03, 0.70, 0.38, and 0.31 for uracil, acetophenone, toluene, and naphthalene, respectively.

There are obvious differences between Figs. 7 and 11. The former figure is based on the electrochemical measurements, which provide the relative velocity difference ($\omega^*_{\beta,c}$), and on the coupling theory of eddy diffusion applied to trans-column velocity biases (Eq. (21)). In contrast, the results in Fig. 11 depend on the

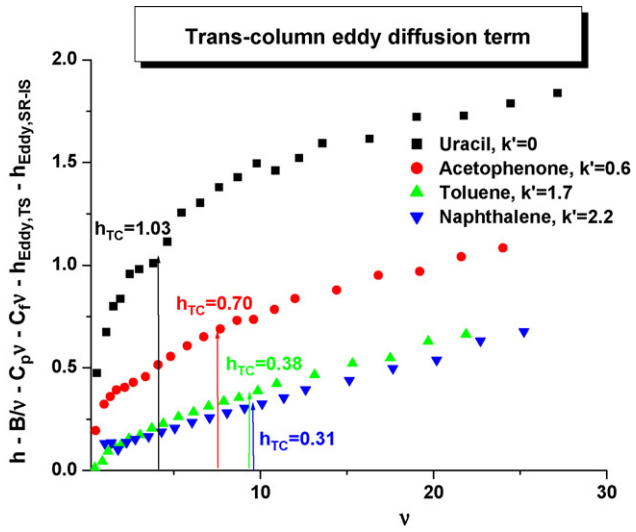

Fig. 11. Plots of the trans-column eddy diffusion term of uracil (squares, $k' = 0$), acetophenone (circles, $k' = 0.7$), toluene (upward triangles, $k' = 1.7$), and naphthalene (downward triangles, $k' = 2.2$) as a function of the interstitial linear velocity. Column 2. Note the significant decrease of the trans-column eddy diffusion term with increasing retention factor. The arrows locate the reduced velocity at which the total HETP is minimum. The estimate of the true relative velocity bias, $\omega^*_{\beta,c}$, was taken as 3.1% for $n = 12$.

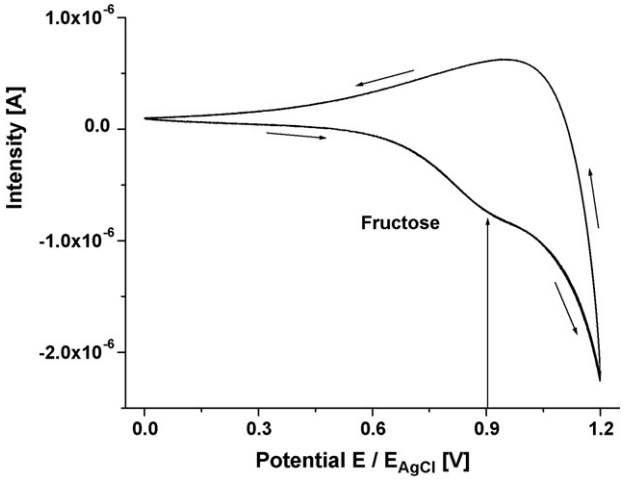

Fig. 12. Voltamperometric cycle of fructose (0.1 M) in water containing 50 mM potassium chloride. Note that the oxidation of fructose can be detected at a *ca.* 0.9 V potential difference between the working electrode and the reference electrode AgCl/Ag.

assumption made on the trans-channel eddy diffusion (idealized 2D-structrue) and on the recent estimate made of the short-range eddy diffusion term in the packed Kinetex column (total pore blocking). The most important result is that both figures are consistent with a significant effect of the retention factor of analytes on the trans-column eddy diffusion and confirm the theoretical demonstration of this effect made earlier in this work.

4.4. How should the true trans-column velocity bias term, $\omega^*_{\beta,c}$ be measured?

The first two sections of this work demonstrated the important influence of solute retention on the trans-column eddy diffusion term in packed columns. Definitely, this term decreases with increasing retention factors. Either one of the two techniques described can be used to estimate the contributions to the column efficiency of the radial flow heterogeneity across this column.

In practice, invasive methods, like measurements of the difference between the outlet migration velocities at the column center and at its wall, should be avoided. The removal of the outlet endfitting and its replacement with a specifically designed frit retainer requires time (at least a few minutes) during which the consolidated bed of particles relaxes, the radial stress decreases, and the external porosity increases. Therefore, the electrochemical measurements are biased to a degree. Furthermore, the working electrode cannot be located exactly at the column wall and measure the eluent migration velocity there, at $r = r_c$, because the extremity of the electrode has a finite size (*ca.* 0.25 mm) and its platinum wire cannot be closer than 0.15 mm from the column wall.

The limitations of the local electrochemical detection method were assessed by using it to measure again the trans-column velocity biases after completion of the HETP measurements. In order to approach as closely as possible the true value of the trans-column velocity biases by local detection, the mesopores of the particles were blocked with liquid n-nonane [2,3], preventing diffusion of the solute through the particle pore volume and minimizing the residence time in the column. We used fructose as the probe solute because this highly polar compound shows no affinity for liquid n-nonane. The eluent was a 50 mM potassium chloride solution

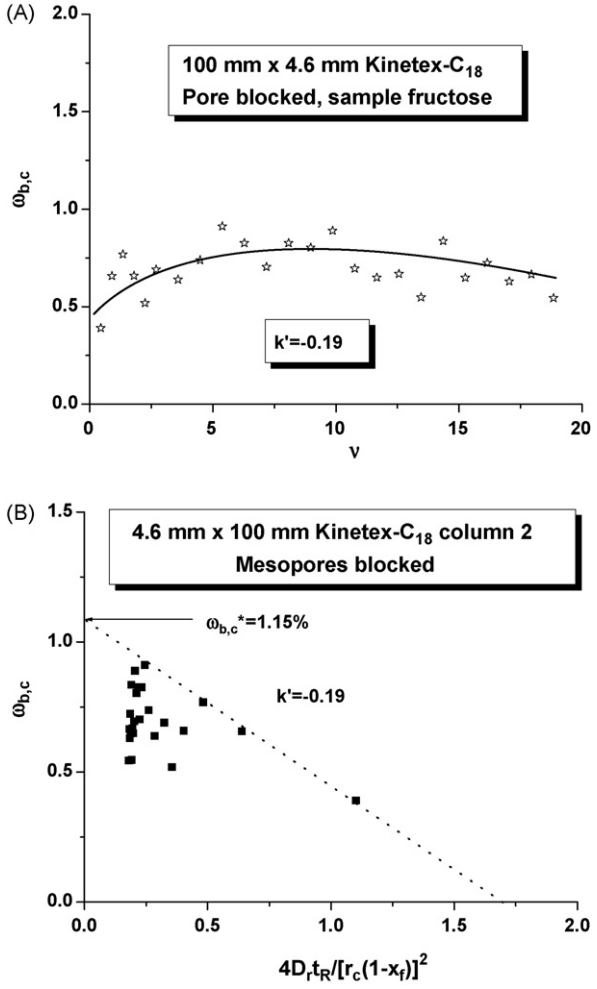

Fig. 13. (A) Plot of the experimental apparent velocity biases, $\omega_{\beta,c}$, of fructose as a function of the reduced interstitial linear velocity of the eluent (H_2O). Access to the mesopore volume was blocked by n-nonane. (B) Same plot as in Fig. 6 but for column 2 with fructose as solute, and mesopore volume inaccessible. Note that the estimate of the true relative velocity bias, $\omega^*_{\beta,c}$, is only 1.1%.

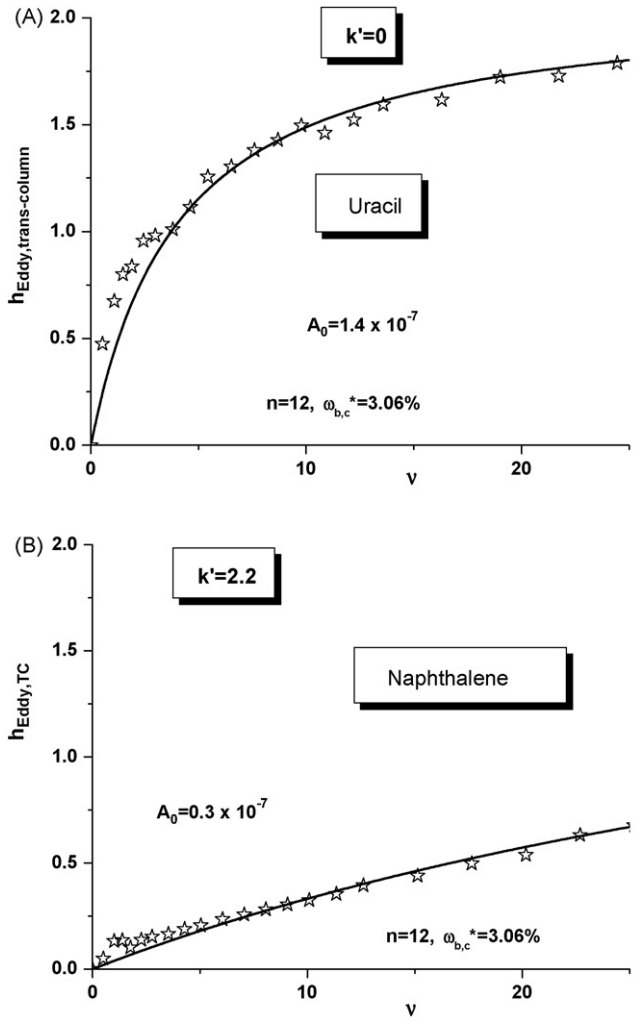

Fig. 14. Comparison between the experimental (empty stars) and the best theoretical (solid line, Eq. (21)) values of the trans-column eddy diffusion term for a non-retained (A, uracil) and a retained (B, naphthalene) compound.

in water. The flow rate was increased from 0.05 (P_{inlet} = 18 bar) to 2.10 mL/min (P_{inlet} = 371 bar). Fig. 12 shows the voltamperogram of fructose and its oxidation at a potential of *ca.* 0.9 V with respect to the reference electrode Ag/AgCl (KCl saturated 3 M). The bulk molecular diffusion coefficient of fructose in pure water is 6.7×10^{-6} cm^2/s, giving a radial dispersion coefficient, $\gamma_e D_m$, equal to 4.2×10^{-6} cm^2/s. The apparent relative velocity biases, $\omega_{\beta,c}$, are plotted in Fig. 13 as a function of the reduced linear velocity. Despite, the relatively moderate precision of the data at high flow rates, it is clear that the velocity biases measured never exceed 1.1% (see Fig. 13B) in this new Kinetex-C_{18} column because static diffusion at low flow rates (D_0) and radial eddies at high flow rates (D_{Eddy}) contribute to relax the radial concentration gradients.

In contrast, if we fit the experimental trans-column eddy diffusion term of uracil in Fig. 11 (full black squares) obtained by fitting the HETP measurements to the general equation Eq. (21) with n = 12, we obtain $\omega^*_{\beta,c} = 3.06\%$ and $A_0 = 1.4 \times 10^{-7}$. As expected, the value of $\omega^*_{\beta,c}$ measured from the HETP data is larger than the value of $\omega_{\beta,c}$ suggested by the LED experiments. Fig. 14A shows the agreement between the experimental data and the general model of trans-column eddy diffusion for uracil. The same graph is shown for the most retained compound, naphthalene, in Fig. 14B.

In conclusion, the non-invasive chromatographic techniques (HETP + peak parking measurements) provides a value for the trans-column velocity bias which is closer to the true value than the one estimated from the LED experiments. Due to experimental limitations, this latter technique underestimates the degree of radial heterogeneity of packed beds.

Our non-invasive chromatographic method is also subject to errors made at low flow rates where the amplitude of the longitudinal diffusion term, B/ν, is large. The general expression of the term B/ν derived from the peak parking method is written [29]:

$$\frac{B}{\nu} = \frac{\Delta\sigma^2}{\Delta t_p} \frac{u_{PP}^2}{1+k_1} \frac{1}{u d_p} \tag{33}$$

where $\Delta\sigma^2/\Delta t_p$ is the slope of the plot of the peak variance *versus* the parking time (with a relative error smaller than a few percent for small molecules) and u_{PP} is the interstitial linear velocity applied in the peak parking experiments (negligible error). Note that the error made on this experimental term does not depend on the error made on the diffusion coefficient, D_m, derived from the Wilke and Chang correlation.

At high flow rates, all the correction terms (B/ν, $C_p\nu$, and $C_f\nu$) are small for small molecular weight compounds. Therefore, the impact of the error made on the expression of C_p (which depends on the external and the shell porosities and on the accuracy of the parallel diffusion model between interstitial and internal volume) and C_f coefficients is negligible.

5. Conclusion

Two series of experiments were conducted in order to demonstrate the fundamental influence of solute retention on the intensity of trans-column eddy diffusion in packed columns. First, local electrochemical detection provided the relative difference of the migration velocities of a solute between the center of the column and a region in the vicinity of its column wall. Evidence was made that the relative velocity bias decreases significantly upon a moderate increase of the retention factor of the solute, from 0 to 3. The radial concentration gradients caused by the radial distribution of flow velocities were completely relaxed for $k' > 3$. The radial distance over which true velocity biases exist was found of the order of 40% of he column radius between r = 1.4 mm and r = 2.3 mm. Second, van Deemter plots were measured in a wide range of reduced linear velocities for four compounds with retention factors between 0 and 3. The HETP curves were corrected for the contributions of longitudinal diffusion (h data at low flow rates), trans-particle mass transfer resistance (peak parking data), external film mass transfer resistance (validated Wilson and Geankoplis correlation), short-range inter-channel velocity biases (combination of local electrochemical detection and total pore blocking experiments), and trans-channel velocity biases (Giddings's theory). The result demonstrated that the residual trans-column eddy diffusion term decreases with increasing retention factor.

The results of the two methods give the same conclusion, the larger the retention factor, the most efficient can the column be. This is not due to either a smaller B term (the B coefficient actually increases with increasing retention factor), a smaller C term (actually, the C term is negligible in all cases), or a significant extra-column band broadening (HETP data were corrected for extra-column contributions). This means that the eddy diffusion A term must be smaller for retained than for non-retained compounds. Because trans-channel eddies are independent of the retention factor, the higher column efficiency obtained for retained compounds in RPLC is directly related to the smaller short-range inter-channel and trans-column eddy diffusion terms for these compounds. Differences are noticeable, however, only for retention factors below 2. No significant difference should be expected for retention factors above 5.

Finally, the real degree of radial flow heterogeneity is better determined by performing HETP and peak parking measurements rather than by using an invasive method such as local detection at column outlet, which underestimates the actual value. From a practical point of view, this work demonstrates that the efficiency of weakly retained solutes is more sensitive to the radial heterogeneity of columns than that of strongly retained ones. A rapid test can be performed to assess the degree of radial heterogeneity of packed beds by measuring the column HETP for non-retained and retained solutes and correcting them for the contributions of longitudinal diffusion, solid–liquid mass transfer resistances, trans-channel and short-range inter-channel eddy diffusion. If the two residual HETPs are markedly different, flow heterogeneities are likely significant. In contrast, if the residual HETPs are nearly distinguishable, the radial flow distribution can be considered as being uniform. The advantage of this method is its non-invasive characteristic. Its inconvenience is that it cannot unambiguously measure the trans-channel, the short-range inter-channel, and the trans-column eddy diffusion terms, but merely provides the overall eddy diffusion term.

List of symbols

Roman letters

A_0	Aris dispersion coefficient
A	eddy diffusion term in the reduced van Deemter Eq. (1)
B	longitudinal diffusion coefficient in the reduced van Deemter Eq. (24)
C_m	Aris coeffient
C_p	trans-particle mass transfer coefficient in the reduced van Deemter Eq. (25)
C_f	external film mass transfer coefficient in the reduced van Deemter Eq. (29)
δ_r	standard radial displacement of the sample during the retention time t_R (m)
d_c	inner diameter of the column tube (m)
d_p	average particle size (m)
D_m	bulk molecular diffusion coefficient (m^2/s)
D_0	apparent diffusion coefficient of the sample in the packed bed immersed with the mobile phase (m^2/s)
$\overline{D_r}$	Average radial dispersion coefficient (m^2/s)
$D_r(x)$	transverse dispersion coefficient at the reduced radial coordinate $x = r/R_c$ (m^2/s)
$D_{eddy}(x)$	contribution of eddy diffusion to the transverse dispersion coefficient at the reduced radial coordinate $x = r/R_c$ (m^2/s)
D_s	surface diffusion coefficient (m^2/s)
$F(\lambda_m)$	pore steric hindrance parameter
F_v	inlet flow rate (m^3/s)
H	total column HETP (m)
h	total reduced column HETP
LED	local electrochemical detection
h_{Long}	reduced longitudinal HETP term
$h_{Eddy,TS}$	reduced trans-channel eddy diffusion HETP term
$h_{Eddy,SR-IS}$	reduced short-range inter-channel eddy diffusion HETP term
$h_{\text{trans-column}}$	reduced eddy dispersion HETP due to trans-column velocity biases
$h_{\text{trans-column,Aris}}$	overall additionnal Aris reduced column HETP generated by heat friction
$h_{\text{trans-column,Flow}}$	overall additionnal flow reduced column HETP generated by heat friction
I_1	scalar given by integral Eq. (12)
I_2	scalar given by integral Eq. (13)
I_3	scalar given by integral Eq. (14)
K_{shell}	Henry's constant of adsorption on the walls of the porous shell
k'	retention factor
k_f	external film mass transfer coefficient (m/s)
k_1	zone retention factor in a core–shell particle
L	column length (m)
l_i	characteristic length of a source i of flow heterogeneity in packed beds (m)
n	parameter in the polynomial Eq. (2) describing the radial flow distribution
p	integer
q	integer
P_{inlet}	system inlet pressure (Pa)
r	radial coordinate (m)
r_c	column inner radius (m)
Sh	Sherwood number
t_p	parking time (s)
t_R	retention time (s)
t_{center}	elution time measured at the column center in LED experiments (s)
t_{wall}	elution time measured st the column wall in LED experiments (s)
u	interstitial linear velocity (m/s)
$u(0)$	interstitial linear velocity at the center of the column $x = 0$ (m/s)
$u(x)$	interstitial linear velocity at the reduced radial coordinate $x = r/r_c$ (m/s)
u_{pp}	interstitial linear velocity in the peak parking experiments (m/s)
$u_R(x)$	migration linear velocity at the reduced radial coordinate $x = r/r_c$ (m/s)
V_c	volume of the column tube (m^3)
x	reduced radial coordinate
x_f	critical radial coordinate below which the flow distribution is uniform
x'	dummy variable in integral Eq. (15)

Greek letters

α	structural parameter of the porous material
ε_e	external column porosity
$\varepsilon_{p,shell}$	porosity of the porous shell
ε_t	total column porosity
γ_e	external obstruction factor
γ_r	radial dispersion parameter associated to a convective process
$\gamma_{p,shell}$	internal obstruction factor of the porous shell
λ_m	ratio of the hydrodynamic radius of the analyte to the mesopore radius
λ_i	eddy dispersion coefficient related to a flow exchange mechanism for a velocity bias of type i
ν	reduced interstitial linear velocity of the eluent to the particle diameter d_p and bulk molecular diffusion coefficient D_m
ω_i	eddy dispersion coefficient related to a diffusion exchange mechanism for a velocity bias of type i
$\omega^*_{\beta,c}$	true relative velocity difference between the center and the wall of the column tube
$\omega_{\beta,c}$	experimental and apparent relative velocity difference between the center and the wall of the column tube measured by LED
Ω	ratio of the intraparticle diffusivity of the sample through the porous shell to the bulk diffusion coefficient
$\phi(x)$	Dimensionless sample migration linear velocity at the radial coordinate x
$\Phi(x)$	Function given by the integral Eq. (15)

$\psi(x)$ Dimensionless radial diffusion coefficient at the radial coordinate x

ρ ratio of the diameter of the solid core to that of the core–shell particle

σ^2 peak variance recorded in the peak parking method (s^2)

Acknowledgements

This work was supported in part by grant CHE-06-08659 of the National Science Foundation and by the cooperative agreement between the University of Tennessee and the Oak Ridge National Laboratory. We thank Tivadar Farkas (Phenomenex, Torrance, CA, USA) for the generous gift of the Kinetex columns and their modified outlet endfittings used in this work and for fruitful discussions.

References

[1] F. Gritti, G. Guiochon, AIChE. J. doi:10.1002/aic.12280.
[2] F. Gritti, G. Guiochon, AIChE. J. doi:10.1002/aic.12271.
[3] F. Gritti, G. Guiochon, AIChE J. 56 (2010) 1495.
[4] D. Cabooter, F. Lynen, P. Sandra, G. Desmet, J. Chromatogr. A 1157 (2007) 131.
[5] J. Giddings, Dynamics of Chromatography, Marcel Dekker, New York, NY, 1965.
[6] B.G. Yew, J. Ureta, R.A. Shalliker, E.C. Drumm, G. Guiochon, AIChE J. 49 (2003) 642.
[7] D. Hlushkou, U. Tallarek, J. Chromatogr. A 1126 (2006) 70.
[8] J. Knox, L. McLaren, Anal. Chem. 36 (1964) 1477.
[9] U. Tallarek, K. Albert, E. Bayer, G. Guiochon, AIChE J. 42 (1996) 3041.
[10] U. Tallarek, K. Albert, G. Guiochon, J. Am. Chem. Soc. 120 (1998) 149.
[11] T. Farkas, M.J. Sepaniak, G. Guiochon, AIChE J. 43 (1997) 1964.
[12] J. Abia, K. Mriziq, G. Guiochon, J. Chromatogr. A 1216 (2009) 3185.
[13] F. Gritti, I. Leonardis, J. Abia, G. Guiochon, J. Chromatogr. A 1217 (2010) 3219.
[14] R. Aris, Proc. Roy. Soc. A235 (1956) 67.
[15] F. Gritti, M. Martin, G. Guiochon, Anal. Chem. 81 (2009) 3365.
[16] F. Gritti, G. Guiochon, Anal. Chem. 78 (2006) 5329.
[17] K. Miyabe, S. Takeuchi, Ind. Eng. Chem. Res. 37 (1998) 1154.
[18] M. Martin, G. Guiochon, Anal. Chem. 54 (1982) 1533.
[19] F. Gritti, G. Guiochon, J. Chromatogr. A 1217 (2010) 1485.
[20] C. Wilke, P. Chang, AIChE J. 1 (1955) 264.
[21] B. Poling, J. Prausnitz, J. O' Connel, The Properties of Gases and Liquids, 5th ed, McGraw-Hill, New York, NY, 2001.
[22] K. Nishida, Y. Ando, H. Kawamura, Colloid Polym. Sci. 261 (1983) 70.
[23] G. Guiochon, A. Felinger, A. Katti, D. Shirazi, Fundamentals of Preparative and Nonlinear Chromatography, 2nd ed., Academic Press, Boston, MA, 2006.
[24] K. Kaczmarski, G. Guiochon, Anal. Chem. 79 (2007) 4648.
[25] E. Wilson, C. Geankoplis, J. Ind. Eng. Chem. (Fundam.) 5 (1966) 9.
[26] K. Miyabe, M. Ando, G. Ando, N. Guiochon, J. Chromatogr. A 1210 (2008) 60.
[27] K. Miyabe, Y. Kawaguchi, G. Guiochon, J. Chromatogr. A 1217 (2010) 3053.
[28] F. Gritti, I. Leonardis, D. Shock, P. Stevenson, A. Shalliker, G. Guiochon, J. Chromatogr. A 1217 (2010) 1589.
[29] F. Gritti, G. Guiochon, J. Chromatogr. A 1217 (2010) 5137.